On the Effects of the External Surface on the Equilibrium Transport in Zeolite Crystals

N. E. R. Zimmermann,*,† B. Smit,‡ and F. J. Keil†

Chemical Reaction Engineering, Hamburg University of Technology, Eissendorfer Str. 38, 21073 Hamburg, Germany, and Department of Chemical Engineering and Department of Chemistry, University of California – Berkeley, 1018 Gilman Hall, Berkeley, CA 94720-1462, USA

E-mail: nils.zimmermann@tu-harburg.de

†Hamburg University of Technology
‡University of California – Berkeley

1 NVT and the Lowe-Andersen thermostat for interface-fluid collisions

In molecular dynamics (MD) simulation studies of confined fluid diffusion, the question whether the rigid-lattice assumption is reasonable still seems to be open.[1,2] Recently, Zimmermann et al. have shown that available force fields can induce significant changes to both the lattice structure and the dynamics of the hopping process of the adsorbates, so that the self-diffusion coefficient is distorted.[1] Since Newsome and Sholl have shown that it is yet very important to account for the energy exchange between fluid molecules at the *external* surface in simulation studies of thin zeolite membranes,[3] an appropriate treatment must be ensured. Jakobtorweihen et al. have, for carbon nanotubes (CNTs), shown that fluid thermalization induced by vibrating pore atoms can be modeled by means of a stochastic thermostat – the Lowe-Andersen thermostat for interface-fluid collisions (LA-IFC).[4] Therefore, it was decided to model the energy exchange of fluid molecules with the lattice oxygen atoms with the LA-IFC thermostat *throughout* the crystal, i.e., at the external surface *and* inside the bulk zeolite.

The parameters neccessary for using the thermostat – the collision cutoff radius, $r_{\text{LA}-\text{IFC}}^{\text{cutoff}}$, and the collision frequencies in x, y, and z, Γ – were roughly estimated from Ref. 5 on basis of pore-size comparison: $r_{\text{LA}-\text{IFC}}^{\text{cutoff}} = 3.6$ Å, and $\Gamma_{x,y,z} = 10^{11}$ s^{-1}. Additionally, tests in a *periodic* AFI crystal (methane and ethane at 300 K and infinite dilution) have been performed in order to check the validity of the parameters. On the one hand, the collision frequencies should be chosen as large as possible in order to allow for efficient energy exchange at the crystal surface. On the other hand, too large a Γ will result in too much decorrelation of the fluid particle dynamics by unrealistically many collisions which, in turn, will lead to a significant decrease in D_{S}.[1] This effect would be most prominent when there are no other adsorbate molecules around it, i.e., at infinite dilution. As can be seen from Figure S1, the collision frequencies are small enough to neither change the free-energy profile nor alter D_{S}, as compared to simulations with a Nosé-Hoover chain[6] thermostat. It, however, must be pointed out that the resulting self-diffusion coefficients from MSD and TST

differ (κ=1, hence no recrossings at infinite dilution observed). The MSD-D_S is larger by a factor of 2.4 and 2.7 for methane and ethane, respectively. Therefore, in the following two paragraphs we shall justify the methodology used in the present study.
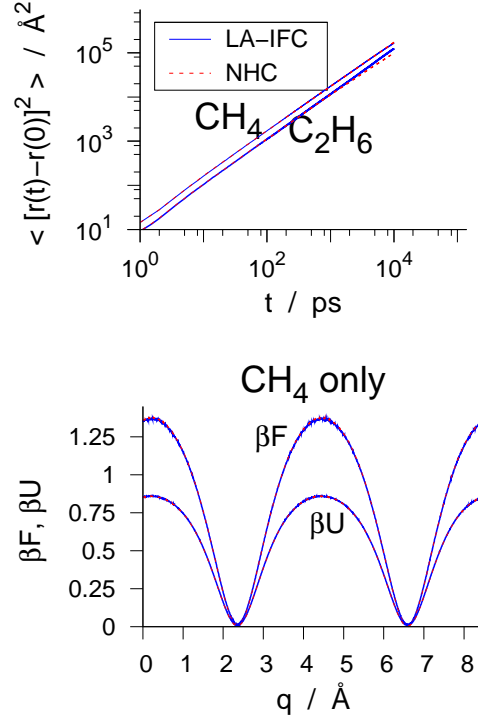

Figure S1: Mean-squared displacement, $\langle[r(t)-r(0)]^2\rangle$, over time, t, (top, methane *and* ethane) and free-energy as well as potential-energy profile of tagged molecules as a function of reaction coordinate, $q = z^{\text{unit cell}}$, (bottom, methane *only*). The simulations were conducted in a periodic all-silica AFI crystal at 300 K and infinte dilution. The two different thermostats – Nosé-Hoover chain[6] (NHC) and Lowe-Andersen thermostat for interface-fluid collisions[4] (LA-IFC) – yield essentially the same results.

The larger MSD-D_S gives rise to a large fraction of multijumps in the bulk zeolite. The dcTST method, however, only accounts for short-term correlations by means of the transmission coefficient (negative back correlations: $\kappa \leq 1$). A first-passage time approach also only captures those short-term correlations, and gives equivalent correlation factors as compared to the dcTST-κs, see Figure 8 in the main article. In fact, multijumps mean that random walk theory is violated which is the basic assumption of dcTST but also for self diffusion in general (sampling the MSD). Surprisingly, the MSD is yet proportional to time, t. For methane self diffusion in an AFI-type zeolite

it is well-known that the system exhibits a system-size effect at finite loadings (see, for example, Refs. 1, and 7). One may speculate that this system-size effect at finite loadings is related to the violation of random walk theory. So, as long as it is not clear whether this system-size effect, and thus the multijumps, is an artifact of the simulations (i.e., MSD sampling in systems with low energy-barriers) or a real phenomena that can be evidenced by experiments, we believe it is better to "impose" a random walk by using the dcTST methodology (or, equivalently, a first-passage times approach) to calculate the tracer transport properties of interest.

Furthermore, we are not aware of methodologies other than or equivalent to (dc)TST, and first-passage time to quantify the *tracer* transport at the crystal surface. Note, that we have checked the one-way-flux method, as, for example, used by Newsome and Sholl,[3] and found that the fluxes are exactly equal to the pure TST fluxes. If the MSD-D_S were used together with a quantity for the tracer surface transport that was based on either of the methods mentioned, this would be an unfair comparison because the MSD-D_S includes not only short-term back correlations but also positive (or, enhancing) multijump correlations; the surface quantity, however, would at best include negative back correlations. From our point of view, it would be neither a fair comparison if we were to use a dual-control volume approach, i.e., a gradient-based method, for determining a surface permeability because we would compare a collective/Fickian transport property (α), with a diffusion coefficient of a single tagged molecule (D_S^{MSD}). Finally, we conclude that it is very reasonable to use the dcTST methodology for comparing the extent of transport in the two regions of interest (bulk zeolite and at the crystal edges) because the *same kind of correlations* (recrossings) are taken into account.

2 Dynamically corrected Transition State Theory

In the following the application of dynamically corrected transition state theory to transport processes of adsorbate molecules confined inside zeolites is described and discussed in detail.

2.1 Free-energy contribution

Small hydrophobic molecules confined in highly siliceous zeolite structures reside preferentially at sites with no or little electric field. These sites usually follow directly from the crystal structure being the cages. The self-diffusive motion of molecules confined in such structures can be regarded as a cascade of infrequent random hops from one cage to an adjacent one. Thus, the validity of applying TST to diffusion problems is fundamentally based upon the assumption of the applicability of random-walk theory, and a large separation of time scales must be observable. In order to quantify the random walk, the probability of an elementary hop has to be computed.

When a molecule attempts to leave a cage, it must traverse through a window in order to reside at an adjacent cage. Therefore, the connection from one cage center to an adjacent one can be used to describe the process of such an elementary hop attempt. It is called reaction coordinate, q. In the following it is assumed that the center-of-mass of the *whole* molecule identifies q rather than one specific atom or bead in case of molecules comprised of several united atoms, compare, for example, Ref. 8.

Three functions are introduced to characterize whether the molecule is in cage A (original cage), n_A, in cage B (target cage), n_B, or in the window (transition state), $n^{\ddagger}$,

$$n_A = H(q^{\ddagger} - q), \tag{1}$$

$$n_B = H(q - q^{\ddagger}), \text{ and} \tag{2}$$

$$n^{\ddagger} = \delta(q^{\ddagger} - q). \tag{3}$$

$q^{\ddagger}$ denotes the position of the transition state (window region). H is the Heaviside function ($H(x) = 1$ for $x \geq 0$ and $H(x) = 0$ otherwise), and δ represents the Dirac delta function ($\delta(0) = \infty$ and $\delta(x) = 0$ otherwise). On the basis of these functions, the relative probabilty, $P_{\in A}(q^{\ddagger})$, of finding

the tagged molecule, that has come from cage A, in the window region, $q^{\ddagger}$, can be obtained from

$$P_{\in A}(q^{\ddagger}) = \frac{\langle n^{\ddagger} \rangle}{\langle n_A \rangle}. \tag{4}$$

Angular brackets denote ensemble averages. The functions, for a closed system,[9] can be expressed in terms of free energies, $F(q)$, of the single tagged molecule yielding

$$P_{\in A}(q^{\ddagger}) = \frac{e^{-\beta F(q^{\ddagger})}}{\int\limits_{\text{cage A}} e^{-\beta F(q)} dq}. \tag{5}$$

where $\beta = 1/(k_B T)$, with T being the absolute temperature of the system and k_B Boltzmann's constant. The probability, $P_{\in A}(q^{\ddagger})$, is thus proportional to the free-energy difference between transition state and cage A. The value of $P_{\in A}(q^{\ddagger})$ is strongly influenced by the choice of the transition state location. It should be chosen such to maximize $\Delta F = F(q^{\ddagger}) - F(q_A)$, whereby q_A denotes the position of the center of cage A.

Since the free-energy profile depends upon the zeolite-adsorbate system, but, for one and the same system, also changes with loading, θ, different probabilities, $P_{\in A}(q^{\ddagger})$, will, in general, be found at different loadings. Also, the temperature has an impact on the free-energy profile. Hence $F(q)$ is in fact $F(q, \theta, T)$, and $P_{\in A}(q^{\ddagger}) = P_{\in A}(q^{\ddagger}, \theta, T)$. It is worthwhile to note that there are several schemes for extrapolating $F(q, \theta, T_1)$ to $F(q, \theta, T_2)$, see for example Ref. 10 and references therein.

The free-energy profile can be obtained from either Widom particle insertion (WPI) or histogram sampling (HS). The latter was used in the present work, because WPI is known to give errorneous results at higher densities.[11,12] From the histogram points, that represent the residence probability of the tagged molecule at a given value of q, $P(q)$, the free-energy is computed by

$$\beta F(q) = -\ln[P(q)], \tag{6}$$

where $\beta = 1/(k_B T)$ and k_B is Boltzmann's constant. Figure S2 summarizes the procedure schem-
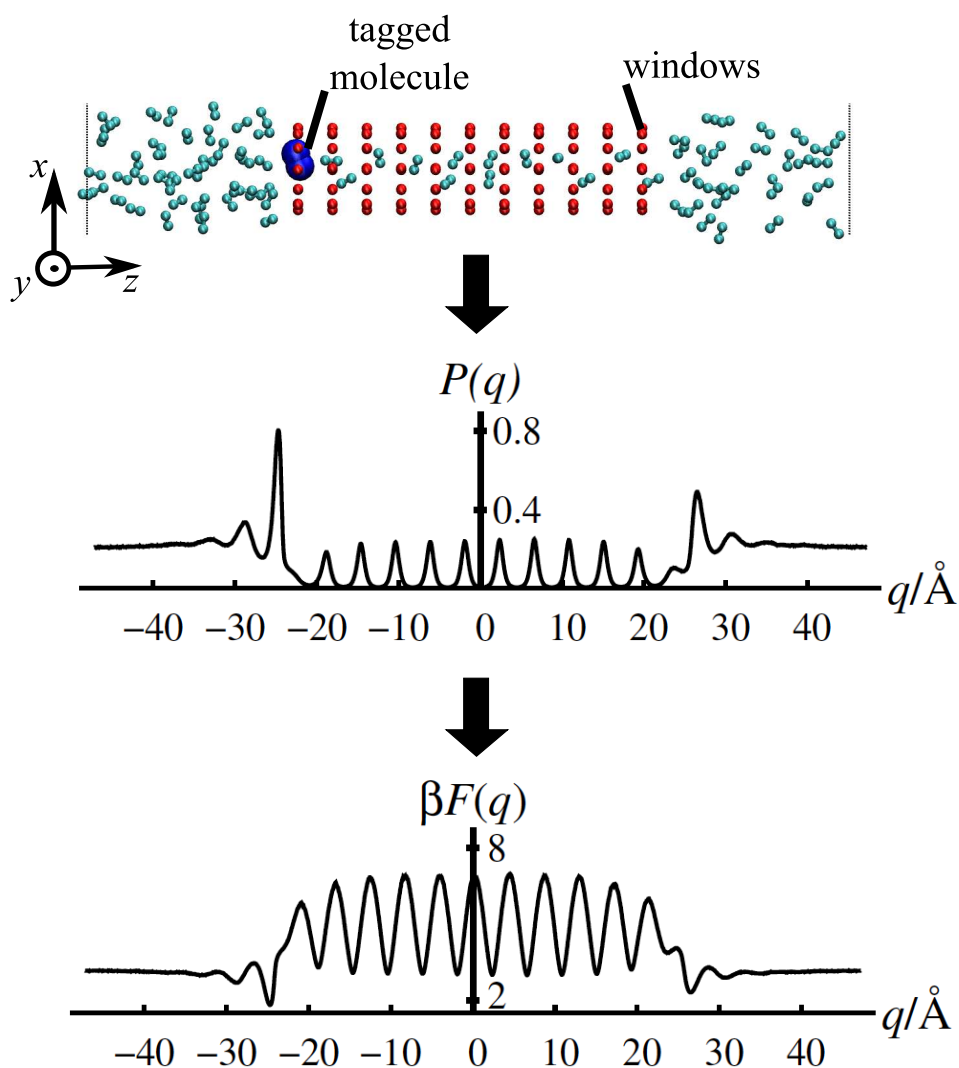
atically.

Figure S2: (Top) Snapshot of a section of the simulation box. The tagged ethane molecule is indicated by large blue spheres. (Center) Histogram along q. (Bottom) Resulting free-energy profile along q.

2.2 Flux contribution

Thus far, the mere probability of finding a molecule at the transition state has been determined. In order to obtain hopping frequencies the time frame involved has to be assessed. It is composed of two contributions: the average uncorreted flux through the dividing surface and a correction factor that accounts for spurious crossings.

By assuming that the velocity of the tagged molecule follows a Maxwell-Boltzmann distribution, the average flux at the transition state, $\langle 0.5 \cdot |\dot{q}| \rangle_{q^{\ddagger}}$, can be estimated to $\sqrt{\frac{k_B T}{2\pi m}}$, where $\dot{q}$ denotes the time derivative of q, i.e., the velocity of the tagged molecule projected onto q, and m the molecule's mass. The TST hopping frequency, $k_{A\rightarrow B}^{TST}$, is thus

$$k_{A\rightarrow B}^{TST} = \sqrt{\frac{k_B T}{2\pi m}} \cdot P_{\in A}(q^{\ddagger}). \tag{7}$$

The tacit assumption in the above equation is that, once a molecule reaches the bottleneck to its hopping attempt, the conventional TST predicts that, provided the molecule has a velocity that points toward the target cage, it will eventually equilibrate therein. However, it could be shown,[8,12,13] that this must not be true per se. Hopping molecules may, particularly at finite loadings, have some likelihood to recross the transition state before having reached q_B. In words of transition path sampling, this trajectory is not reactive because it does not connect state A with state B. The pure TST frequency is therefore an upper bound for the true frequency, $k_{A\rightarrow B}$. The introdcution of the so-called transmission coefficient[9,14] defined as

$$\kappa \equiv \frac{k_{A\rightarrow B}}{k_{A\rightarrow B}^{TST}} \tag{8}$$

gives the correction to those unsuccessful hopping attempts. When the choice of the reaction coordinate is not optimal, because q is, in general, a function of the *entire* configuration space ($q = q(\mathbf{r_1}, ..., \mathbf{r_N})$), κ will additionally be the *exact* correction to this maldefinition.[9]

The transmission coefficient is usually identified as the plateau value of the reactive flux correlation function (RFCF) defined as[9,11,14]

$$\kappa(t) = \frac{\left\langle \dot{q}(0) \cdot H[q(t) - q^{\ddagger}] \cdot \delta[q(0) - q^{\ddagger}] \right\rangle}{\left\langle 0.5 \cdot |\dot{q}(0)| \right\rangle}, \tag{9}$$

where $q(0)$ and $\dot{q}(0)$ denote the initial ($t = 0$) position and velocity of the molecule in terms of

the reaction coordinate, respectively. This time-dependent correlation function can be interpreted as the velocity-wise ($\dot{q}(0)$) weighted likelihood that, after some time t, a molecule that has started its trajectory in the window region ($\delta[q(0) - q^{\ddagger}]$) with a velocity toward the target cage B (0.5 in denominator of eq. 9) has already reached B.

The correlations encompassed are short-term correlations occuring during the jump. These are usually backcorrealations due to particle-particle interactions. At some finite loading, it is very likely that a molecule attempting to reside in the new cage B hits on another adsorbate molecule. Hence the probability to jump back to the old cage is high because that cage is almost certainly empty. The plateau value of the RFCF, κ^{plat}, is therefore attained in a time, $\tau^{\text{mol}} \approx |q_{\text{A}} - q^{\ddagger}|/\langle|\dot{q}|\rangle$, much shorter than the average reaction time, $\tau^{\text{rxn}} = (k_{\text{A}\rightarrow\text{B}} + k_{\text{B}\rightarrow\text{A}})^{-1}$. This time is *not* expected to be a *constant*, as loading increases,[9] because a new time frame, τ^{coll}, as a consequence of increasing molecular collisions will set in and most likely retard κ^{plat}. At this point it should be pointed out that other correlations, such as cooperative jump phenomena and concerted motion of clusters, can occur in case of fluid molecules diffusing through confined nanopores, see for example Refs. 15–17. We believe however that those are not of significance to this study, because rather small molecules are considered as compared to Ref. 17. Moreover, the molecules do neither diffusive through entirely smooth pores (compare Ref. 15), nor do they undergo single-file behaviour (compare Ref. 16).

The RFCF, as indicated by the ensemble brackets, is to be computed for many starting configurations that are distributed according to the Boltzmann distribution. For harvesting these starting configurations, a modified version of the BOLAS[18] algorithm, called equilibrium path sampling[19] (EPS), was used. As has been shown in Ref. 18, the configurations sampled by BOLAS/EPS are distributed according to the equilibrium distribution. Using the BOLAS/EPS method for sampling starting configurations yet causes some problems at low loadings. As the density is low and the shoots quite short (200...300 fs), it is sampled in a region of configuration space that is too correlated. Therefore, there is an imperative for generating starting configurations from several independent runs where the BOLAS/EPS starts with totally different initial configurations. At

intermediate loadings this problem levels off.

When, during the execution of a separate shoot for the RFCF at time t^{stop}, the tagged molecule reaches either of the free-energy basins before the correlation time is attained (t^{correl} =maximum sampling time for the RFCF), the shoot is stopped and the remaining entries of the $\kappa(t)$-function for $t \leq t^{\text{correl}}$ updated with $\dot{q}(0)$ of the current shoot and $H[q(t^{\text{stop}})]$. This procedure ensures that only short-term correlations are accounted for in κ^{plat}. The RFCFs for the intracrystalline hoppings were, for convenience, computed in a fully periodic crystal rather than in the membrane-like crystal used for studying the surface transport. For those short-term correlations which are governed by the RFCF, the results will be the same.

Figure S3 illustrates the procedure of the RFCF simulations (here: at the crystal surface). The starting configurations (transition state) are initialized with velocities and then integrated forward in time (v^{forward}), either until the correlation time has exceeded or, as is the case in the example, the tagged molecule has reached one of the regions that correspond to the free-energy basins, top of Figure S3. Then the velocities of *all* beads are reversed and the system is integrated backward in time. In fact, two RFCFs are computed: one that identifies the free-energy basin left from the transition state (TS) as target or product state ($q = -z$), and the other one that aims toward the basin right from the TS ($q = +z$), see also bottom of Figure S3.

2.3   Flux density

Dynamically corrected transition state theory originates from the consideration of a reversible monoatomic chemical reaction

$$A \underset{k_{\text{B}\to\text{A}}}{\overset{k_{\text{A}\to\text{B}}}{\rightleftharpoons}} B.$$
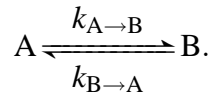
The phenomenological rate law

$$\frac{\mathrm{d}n_{\text{A}}(t)}{\mathrm{d}t} = -k_{\text{A}\to\text{B}} \cdot n_{\text{A}}(t) + k_{\text{B}\to\text{A}} \cdot n_{\text{B}}(t) \tag{10}$$
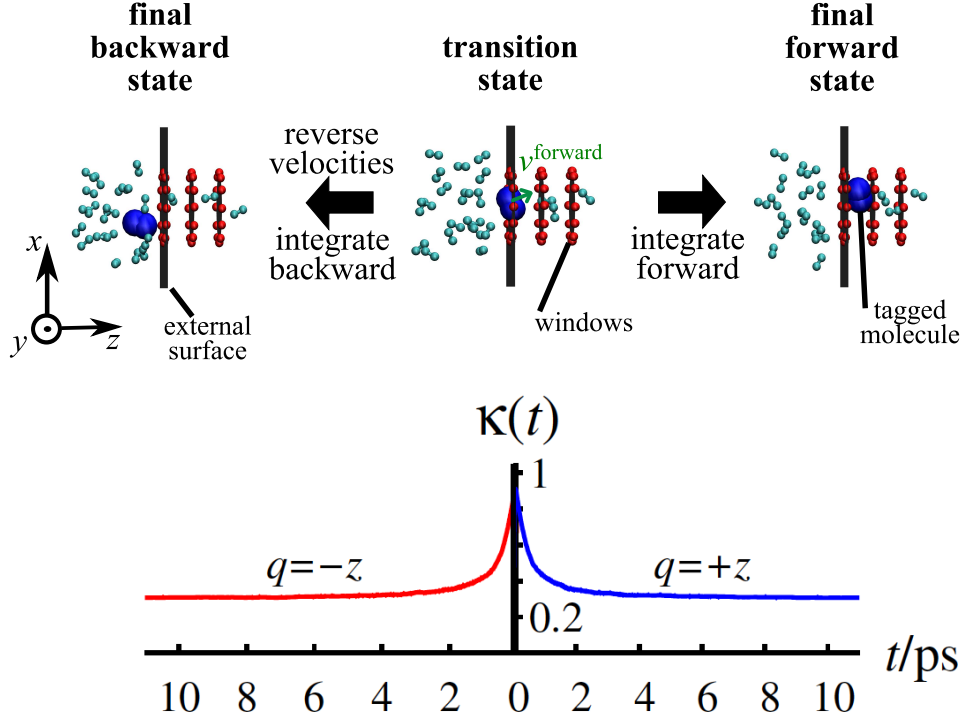
Figure S3: (Top) Snapshots from a reactive flux correlation function (RFCF) simulation. The tagged ethane molecule is indicated by large blue spheres. (Bottom) Final RFCF, $\kappa(t)$, for the adsorption ($q = +z$) and desorption process ($q = -z$), respectively.

is assumed to be valid. From detailed balance follows that, in equilibrium, following relation holds:

$$k_{A \to B} \cdot \langle n_A \rangle = k_{B \to A} \cdot \langle n_B \rangle, \text{ with} \tag{11}$$

$$\langle n_A \rangle = \frac{\int\limits_{A} e^{-\beta F(q)} dq}{\int\limits_{A+B} e^{-\beta F(q)} dq}, \text{ and} \tag{12}$$

$$\langle n_B \rangle = 1 - \langle n_A \rangle. \tag{13}$$

This is a very important realization for asymmetric barriers. In periodic crystal studies[8,12,13] the free-energy barriers have been symmetric and $k_{A \to B}$ and $k_{B \to A}$ have thus been identical. In the case of hoppings at the crystal surface, however, the barriers are, in general, asymmetric and the above equations emphasis the request of identical *rates of change* of species A and B, i.e., identical equilibrium fluxes, rather than identical transmission frequencies, i.e., hopping frequencies.

S11

Because $\langle c_A \rangle = \frac{\langle n_A \rangle}{V_A}$, with $V_A = $ const., the flux density of A through the dividing surface, $j_{A \to B}$, can be computed on basis of the corrected hopping frequency and the average concentration, $\langle c_A \rangle$,

$$j_{A \to B} = \kappa \cdot k_{A \to B}^{\text{TST}} \cdot \langle c_A \rangle \lambda_A. \tag{14}$$

$\langle c_A \rangle \lambda_A$ stems from computing the number of species A (found left from the transition state: $\langle n_A \rangle = \int_{\text{cage A}} \langle c \rangle \cdot dV^*$) and its conversion into flux densities by dividing by the cross sectional area A_A ($dV^*/A_A \to d\lambda^*$). The term $j_{B \to A}$ is obtained in the same way and it must equal $j_{A \to B}$.

3 Transition state locations and free-energy landscapes

The location of the transition state (TS), i.e., the bottleneck to the hopping process, of small hydrophobic adsorbate molecules inside *bulk* zeolites are usually known a priori, because the barriers are mostly entropic in nature and thus follow directly from the crystal structure. Also, the transition states remain usually at the same position when loading increases, see Figure S4, as well as Refs. 1, and 20. The location of the free-energy basins, where the hopping molecule spends much time in, does not change either. As for the surface hoppings studied in this work, the situation is different. Although the location of the free-energy basin for both sides (gas-space and zeolite-space side) remain stable for one and the same crystal side (window-wise $\leftrightarrow$ cage-wise truncation), the location of the transition states, i.e., where the free energy reaches its local maximum in the vicinity of the outmost crystal atoms, changes with increasing number of molecules inserted into the simulation box, see Figure S5. Initially, the TS is located outwards with respect to the anticipated barrier location, i.e., the position of the outmost window atoms. The reason is, most likely, that fluid molecules that try to desorb must overcome a huge potential-energy barrier, particularly at low loadings, θ. Since this influence is very strong, the location of the potential-energy barrier determines the location of the free-energy barrier at low θ. In contrast to the F-profiles which are flat if θ is low, the U-profiles are sharply peaked. By inserting more and more molecules into the simulation box, a gentle but definite inward shift of the TS is observable. As the ultimate TS

location is the anticipated entropic barrier, there, in consequence, seem to be 2 mechansims that compete with each other:

1. The energetic more favorable situation to be as deeply adsorbed into the pores as possible. This influence renders it more favorable for the fluid molecules to yet not be entirely adsorbed, i.e. having yet not passed the entropic barrier, than being adsorbed in the free-energy basin at the external surface.

2. The anticipated entropic barrier that becomes dominating when the pores and the external surface are crowded, this is, at high loadings.
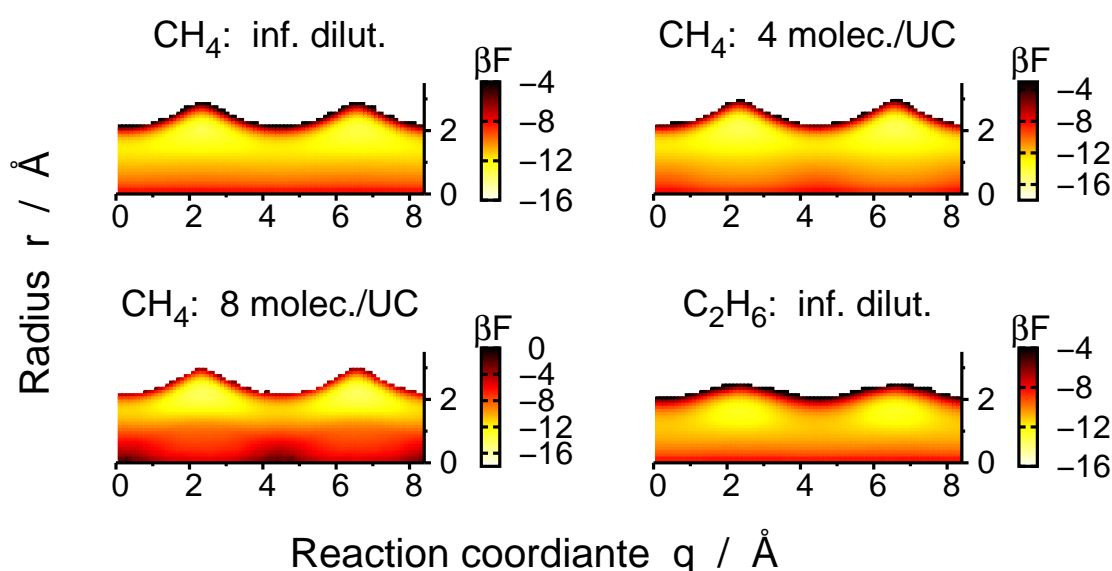

Figure S4: Two-dimensional free-energy landscapes, $\beta F(q,r)$, of methane and ethane inside a periodic AFI crystal (300 K, various loadings). The radius, r, is the distance of the tagged molecule from the pore center. The colorbox range is chosen such that white areas indicate regions that were never visited by the molecules. The F-landscapes show that ethane "feels" a less corrugated wall than methane because it is bulkier than methane.

The *gentle* shift is observable for the window-wise truncated crystal *only*. As for the cage-wise truncation, there is a "first order transition" of the barrier location. In contrast to the window-truncated side, where U-barrier and the F-barrier location were quite close to each other and, thus, has led to the gentle, "smeared" transiton of the TS location, the large separation between the

maximum in the U-profile and F-profile leads to a sharp transition, i.e., at some given loading one of the two mechanisms described above is entirely dominating the bottleneck location.
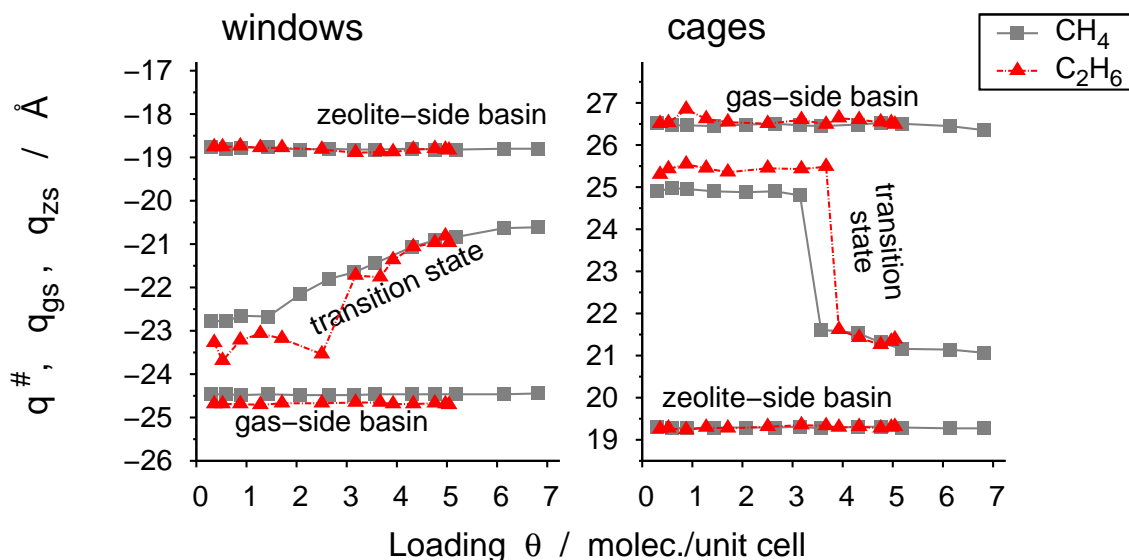

Figure S5: Location of the transition state, gas-side basin and zeolite-side basin, $q^{\ddagger}$, q_{gs}, and q_{zs}, respectively, in the surface regions as functions of loading, θ, for metahne and ethane and both truncation realizations (AFI surface, 300 K).

The usual path of hopping molecules that are confined in the bulk zeolite is close to the pore walls, as evidenced by the 2D-free-energy landscapes in Figure S4. The molecules do hence not adsorb/desorb "straight" from/into the gas phase but first stick to the external surface before proceeding further to either the gas phase or the interior of the pores. When considering the situation at low loading, where the TS at the surface is shifted outwardly, a molecule that tries to desorb thus creeps around the pore mouth and, although it has already made its way well around the concluding oxygen atoms of the pore mouth, it is rather dragged back inside the pore, because, from there, the molecule feels the attractive potential energy still very much in comparison to what lies in front of its desorption path, i.e., on the way toward the external surface.
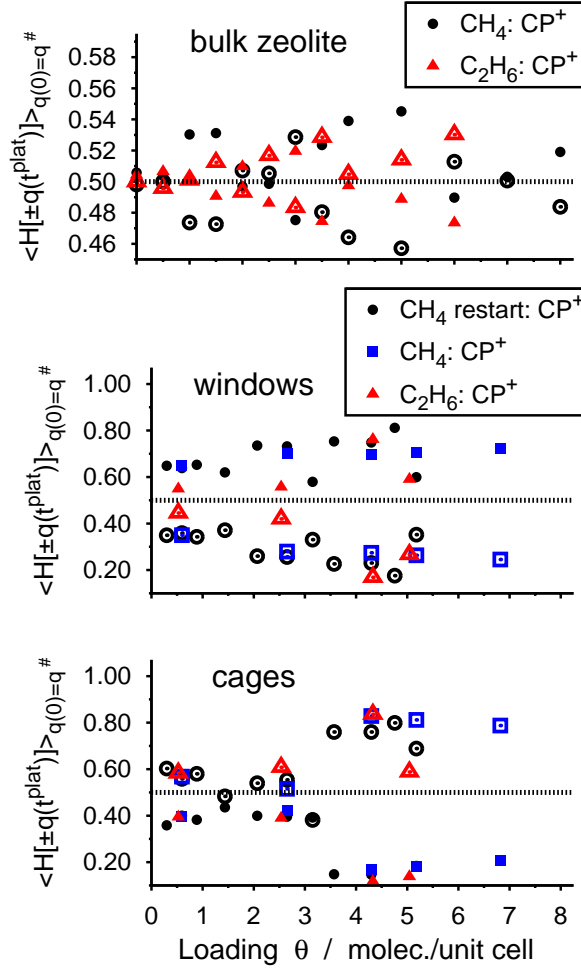
Figure S6: Committor probability of the forward (CP$^+$, filled symbols) shoot, $\langle H[q(t^{\text{plat}})] \rangle_{q(0)=q^{\ddagger}}$, as a function of loading, θ, for methane and ethane in a periodic AFI crystal (top), at the window-wise truncated crystal surface (center), and for the cage-wise truncation (bottom); all 300 K. The committor probability (CP$^-$) of the corresponding backward shoot, $\langle H[-q(t^{\text{plat}})] \rangle_{q(0)=q^{\ddagger}}$, is plotted with open symbols.

4 Committor probability and correlation plots of the RFCF

In Figure S6, the committor probabilities (CPs) obtained from reactive flux correlation function (RFCF) simulations in the bulk zeolite, i.e., intracrystalline hopping, and at the crystal surface, i.e., adsorption/desorption, are plotted. CP gives the "absolute" fraction, i.e., not correlated to

the initial momentum, of those trajectories that were initiated at the transition state ($q(0) = q^{\ddagger}$), and eventually equilibrate either in the product basin, $\langle H[q(t^{\text{plat}})]\rangle_{q(0)=q^{\ddagger}}$, or in the reactant basin, $\langle H[-q(t^{\text{plat}})]\rangle_{q(0)=q^{\ddagger}}$, see also Refs. 21, and 22. In case of the bulk zeolite, the CPs for both sides are equal, as was expected because of the symmetry of the barriers. Furthermore, the values are always close to 0.5 indicating that $\approx$100% of the trajectories have equilibrated in either basin within the correlation time.

The committor probability (CP) for hopping into the zeolite and toward the gas phase are not 0.5. The sum of the CPs at a given crystal end was however always close to unity, indicating that $\approx$100% of the shoots have finished in either free-energy basin within the correlation time chosen. The CP of the adsorption process, CP^{ads}, is always larger than the CP of the corresponding desorption process. Furthermore, CP^{ads} rather increases with loading for the window-wise truncated side, whereas it is initially constant and then jumps abruptly to a larger value between 3 and 4 molecules per unit cell at the cage-wise truncated crystal end. The trend of the CPs and the location-shift of the transition states seem to be correlated. This correlation, together with the seemingly constant κ at high loadings, gave the motivation to conduct additional simulations: RFCF simulations of methane adsorbing/desorbing at the window-wise truncated crystal side at low loading (θ =0.9 molec./unit cell). This time starting configurations were yet harvested in the window region instead of the location of the barrier. This is, in the context of dynamically corrected transition state, legitimate, because it is sufficient to identify the transition state in the *vicinity* of the barrier. κ will then not only account for recrossing, but also be the exact correction to this error source. It turns out, that the transmission coefficient is 0.44 which is very close to the average at high loadings, where the transition state, i.e., the maximum of $\beta F(q)$, is, in fact, found at the location of the window atoms. This further supports the conjecture that the barrier crossing is diffusive at the surface, and, moreover, shows that the extent of diffusive crossings is independent on loading when choosing the last crystal atoms as barrier location.

Distributions of the correlation between success/failure to reach the aimed cage and the tagged particle's initial distance from the pore center as well as its momentum on top of the barrier indicate

three main points for the bulk-zeolite barrier crossing:

1. Those trajectories that recross start predominently farther apart from the pore axis.

2. At high loadings, the initial configuration does not have any influence on the success of the hopping attempt, i.e., whether the trajectory equilibrates in the target cage or not, because there are hardly any initial configurations found close to the pore center.

3. Trajectories with initially low momentum of the tagged molecule have a chance to recross at low loadings only, whereas this continuously shifts to also high-initial-momentum trajectories, as the zeolite becomes more crowded, see Figure S7.

At high loadings the success of a shoot is therefore strongly dependent on the interactions with molecules that have resided in those two cages which the tagged molecule lies initially in-between. These observations hold for both adsorbate types.
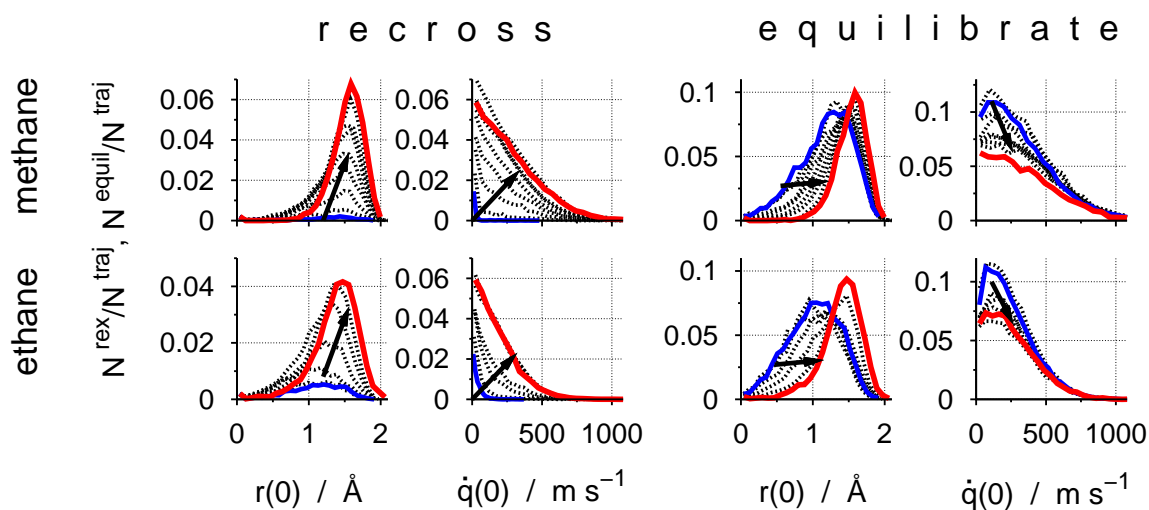

Figure S7: Correlation plots obtained from RFCF simulations in a periodic AFI crystal; top: methane, bottom: ethane. The 4 diagrams on the left correspond to trajectories that have failed to equilibrate in the target cage, the 4 diagrams on the right correspond thus to the successfully equilibrated ones. $r(0)$ denotes the distance of the tagged particle from the pore center at the beginning of the RFCF trajectory, and $\dot{q}(0)$ its initial velocity in z direction. Arrows indicate the evolution of the distributions, as loading, θ, increases. $\theta = 0...8$ molec./unit cell for methane, and $\theta = 0...6$ for ethane, with $\Delta\theta = 1$ molec./unit cell.

The same kind of correlation plots for the surface-barrier crossing do not reveal any indications of what the success of a jump depends on, see Figure S8. Nevertheless, they are a) consistent with the two-dimensional free-energy landscapes and the shift of the transition state in that starting configurations are found at smaller radii when loading is high because of the inward-shift of the transition state where the molecules are then more confined, and b) reflect again the diffusive character of the barrier-crossing process at the surface.
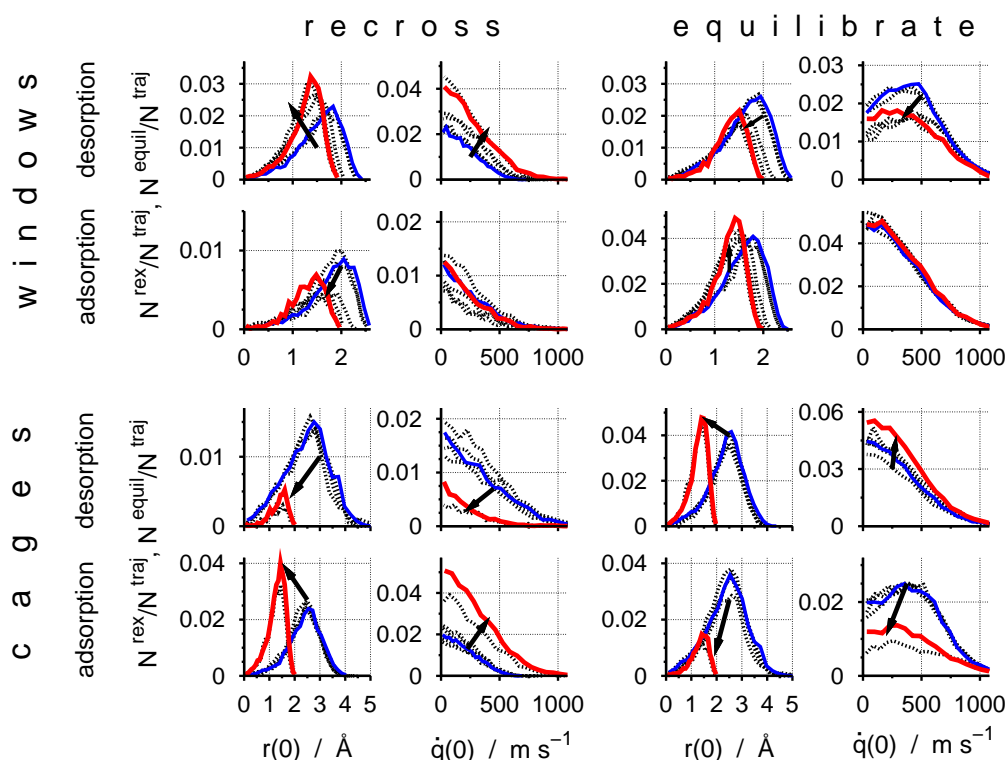

Figure S8: Correlation plots obtained from RFCF simulations initialized at the AFI-crystal surface (methane, 300 K). $r(0)$ denotes the distance of the tagged particle from the pore center at the beginning of the RFCF trajectory, and $\dot{q}(0)$ its initial velocity in z direction. If it was possible the arrows indicate the evolution of the distributions, as loading, θ, increases. $\theta = 0.6, 0.9, 1.4, 2.1, 2.7, 4.3$ and 5.2 molec./unit cell. The thick blue lines and the thick red lines indicate thus the distributions obtained at the lowest loading (0.6), and at the highest loading (5.2), respectively.

References

(1) Zimmermann, N. E. R.; Jakobtorweihen, S.; Beerdsen, E.; Smit, B.; Keil, F. J. *J. Phys. Chem. C* **2007**, *111*, 17370–17381.

(2) Demontis, P.; Suffritti, G. B. *Micropor. Mesopor. Mater.* **2009**, *125*, 160–168.

(3) Newsome, D. A.; Sholl, D. S. *J. Phys. Chem. B* **2005**, *109*, 7237–7244.

(4) Jakobtorweihen, S.; Verbeek, M. G.; Lowe, C. P.; Keil, F. J.; Smit, B. *Phys. Rev. Lett.* **2005**, *95*, 044501.

(5) Jakobtorweihen, S.; Keil, F. J.; Smit, B. *J. Phys. Chem. B* **2006**, *110*, 16332–16336.

(6) Martyna, G. J.; Tuckerman, M. E.; Tobias, D. J.; Klein, M. L. *Mol. Phys.* **1996**, *87*, 1117–1157.

(7) Tepper, H. L.; Hoogenboom, J. P.; van der Vegt, N. F. A.; Briels, W. J. *J. Chem. Phys.* **1999**, *110*, 11511–11516.

(8) Dubbeldam, D.; Beerdsen, E.; Vlugt, T. J. H.; Smit, B. *J. Chem. Phys.* **2005**, *112*, 224712.

(9) Chandler, D. *J. Chem. Phys.* **1978**, *68*, 2959–2970.

(10) Schüring, A.; Auerbach, S. M.; Fritzsche, S. *Chem. Phys. Lett.* **2007**, *450*, 164–169.

(11) Frenkel, D.; Smit, B. *Understanding Molecular Simulations, From Algorithms to Applications*; Academic Press: San Diego, 2002.

(12) Beerdsen, E.; Smit, B.; Dubbeldam, D. *Phys. Rev. Lett.* **2004**, *93*, 248301.

(13) Krishna, C. A.; Yoshanath, S.; Schüring, A.; Kärger, J.; Fritzsche, S. *J. Chem. Phys.* **2009**, *submitted*.

(14) Bennett, C. H. *Thin Solid Films* **1975**, *25*, 65–70.

(15) Bhatia, S. K.; Nicholson, D. *J. Chem. Phys.* **2007**, *127*, 124701.

(16) Sholl, D.; Fichthorn, K. A. *Phys. Rev. Lett.* **1997**, *79*, 3569–3572.

(17) Jobic, H.; Ramanan, H.; Auerbach, S. M.; Tsapatsis, M.; Fouquet, P. *Micropor. Mesopor. Mater.* **2006**, *90*, 307–313.

(18) Radhakrishnan, R.; Schlick, T. *J. Chem. Phys.* **2004**, *121*, 2436–2444.

(19) Peters, B.; Zimmermann, N. E. R.; Beckham, G. T.; Tester, J. W.; Trout, B. L. *J. Am. Chem. Soc.* **2008**, *130*, 17342–17350.

(20) Beerdsen, E.; Smit, B. *J. Phys. Chem. B* **2006**, *110*, 14529–14530.

(21) Du, R.; Pande, V. S.; Grosberg, A. Y.; Tanaka, T.; Shakhnovich, E. S. *J. Chem. Phys.* **1998**, *108*, 334–350.

(22) Bolhuis, P. G.; Chandler, D.; Dellago, C.; Geissler, P. L. *Annu. Rev. Phys. Chem.* **2002**, *53*, 291–318.